Pal 13: its moderately extended low-density halo and its accretion history

Andrés E. Piatti[1,2] and José G. Fernández-Trincado[3]

[1] Consejo Nacional de Investigaciones Científicas y Técnicas, Godoy Cruz 2290, C1425FQB Buenos Aires, Argentina
[2] Observatorio Astronómico, Universidad Nacional de Córdoba, Laprida 854, 5000 Córdoba, Argentina
  e-mail: `andres.piatti@unc.edu.ar`
[3] Instituto de Astronomía y Ciencias Planetarias, Universidad de Atacama, Copayapu 485, Copiapó, Chile

ABSTRACT

We present results based on Dark Energy Camera Legacy Survey (DECaLS) DR8 astrometric and photometric data sets of the Milky Way globular cluster Pal 13. Because of its relatively small size and mass, there is not yet a general consensus on the existence of extra-tidal structures surrounding it. While some previous results suggest the absence of such features, others show that the cluster is under the effects of tidal stripping. We have built a cluster stellar density map from DECaLS g, r magnitudes – previously corrected for interstellar reddening – of stars placed along the cluster main sequence in the color-magnitude diagram. The resulting density map shows nearly smooth contours around Pal 13 out to approximately 1.6 t the most recent estimate of its Jacobi radius, which was derived whilst taking into account the variation along its orbital motion. This outcome favors the presence of stars escaping the cluster, a phenomenon frequently seen in globular clusters that have crossed the Milky Way disk a comparably large number of times. Particularly, the orbital high eccentricity and large inclination angle of this accreted globular cluster could have been responsible for the relatively large amount of lost cluster mass.

Key words. globular clusters: general – globular clusters: individual: Pal 13 – techniques: photometric

1. Introduction

Extended stellar structures have been observed around a significant number of Galactic globular clusters (Carballo-Bello et al. 2012). For instance, Correnti et al. (2011) discovered an extended stellar halo surrounding the distant NGC 5694, while Olszewski et al. (2009) found an unprecedented extra-tidal, azimuthally smooth, halo-like diffuse spatial extension of NGC 1851, and a similar structure was also found around 47 Tuc by Piatti (2017a). Furthermore, long tidal tails have been detected in the fields of NGC 288 (Shipp et al. 2018), NGC 5466 (Belokurov et al. 2006), NGC 7492 (Navarrete et al. 2017), Pal 1 (Niederste-Ostholt et al. 2010), Pal 5 (Odenkirchen et al. 2003), Pal 14 (Sollima et al. 2011), Pal 15 (Myeong et al. 2017), ω Cen (Ibata et al. 2019), and M 5 (Grillmair 2019); and other globular clusters have been found to be embedded in a diffuse stellar envelope extending to a radial distance of at least five times the nominal tidal radius, as in the cae of M 2 (Kuzma et al. 2016), for example. From a theoretical point of view, some N-body simulations show that potential escapers (Küpper et al. 2010) or potential observational biases (Balbinot & Gieles 2018) could contribute to the detection of extended envelopes around globular clusters, among others.

There has been some discussion in the literature about the existence of extra-tidal features around Pal 13. Küpper et al. (2011) performed N-body simulations from which they found that the cluster is most likely near to its apogalacticon and therefore appears supervirial and blown-up, meaning that extra-tidal stars have been pushed back into the vicinity of the cluster. Bradford et al. (2011) obtained an outer surface brightness slope shallower than that for typical globular clusters, suggesting that

at large distances, tidal debris is likely affecting the cluster stellar density profile; according to these latter authors, this could be evidence for tidal stripping. Further results that remain to be reconciled are those derived by Kundu et al. (2019) and Yepez et al. (2019), respectively, using *Gaia* proper motions. While the former authors concluded on the absence of extra-tidal RR Lyrae stars ripped apart from a cluster because of tidal disruption, the latter found that *Gaia* proper motions of cluster members show significant scatter, consistent with tidal stripping. Siegel et al. (2001) also suggested a significant degree of tidal destruction on the basis of various pieces of observational evidence.

It is worth mentioning that the tidal radius of Pal 13 has been attained in several studies, resulting in remarkably different values. For instance, Côté et al. (2002) determined a tidal radius of $r_t = 26' \pm 6'$ from surface density and surface brightness profiles. These latter authors mention that details of background subtraction and model-fitting lead to the suggestion that Pal 13 either contains a substantial population of extra-tidal stars or is considerably more spatially extended than previously thought. Later, Bradford et al. (2011) derived a smaller tidal radius of $r_t = 13.9' \pm 1.5'$ from a maximum likelihood method applied to all stars in a color-magnitude diagram (CMD) selection window, while Sollima et al. (2018) using the same data set and a different analysis method adopted $r_{lim} = 11.2'$. More recently, Baumgardt et al. (2019) estimated $r_t = 4.94'$ by comparing the cluster density profile to a large suite of direct N-body star cluster simulations. We note that the value tabulated in the catalog of Harris (1996, 2010 Edition) is $r_t = 2.19'$.

Massari et al. (2019) associated the origin of the globular cluster Pal 13 to the Sequoia dwarf galaxy, which took part in an early substantial accretion event that contributed to the

formation of the Milky Way stellar halo (Myeong et al. 2019), a scenario also supported by the identification of extended tidal debris with globular-cluster-abundance-like patterns in the inner halo (e.g., Fernández-Trincado et al. 2019). A further six globular clusters have been associated to the same progenitor, namely FSR 1758, IC 4499, NGC 3201, 5466, 6101, and 7006. As far as we are aware, four of them have been found to have extra-tidal features: FSR 1758: Barbá et al. (2019); NGC 3202: Kunder et al. (2014); and NGC 5466, and NGC 7006: Jordi & Grebel (2010).

A recent example of this phenomenon are the globular clusters associated to *Gaia* Enceladus (also known as *Gaia* Sausage), a major accretion event that built the stellar halo of the Milky Way (Belokurov et al. 2018). Indeed, studies of their outer regions have been performed for nine out of ten associated globular clusters and all of them show some of the above mentioned signatures. For instance, NGC 1851, 1904, 2298, and 2808 exhibit tidal tails (Carballo-Bello et al. 2018); extra-tidal features have been found in NGC 362 (Vanderbeke et al. 2015), NGC 7089 (Kuzma et al. 2016) and NGC 6779 (Piatti & Carballo-Bello 2019); and Carballo-Bello et al. (2012) mapped the extended envelopes of NGC 1261 and 6864, respectively.

Here, we exploit the Dark Energy Camera Legacy Survey (DECaLS, Dey et al. 2019) in order to address the issue of the existence of extra-tidal features around Pal 13. Section 2 describes the retrieved data sets, while in Sect. 3 we deal with the construction of the intrinsic cluster stellar density map. A corresponding analysis of the cluster origin and kinematics is explained in Sect. 4. Finally, Sect. 5 summarizes the main outcomes of this work.

2. Data handing

We downloaded all the information available in the DECaLS. DR8[1] catalog for an area of $2° \times 2°$ centered on Pal 13. The retrieved catalog contains 306 454 sources, for which astrometric and photometric data are provided homogeneously. As a quality check, in the subsequent analysis we only kept those sources with morphological model "PSF" (stellar point sources), which resulted ni in errors in the PSF g magnitude and $g - r$ color of less than 0.04 and 0.07 mag, respectively. These upper limits for the photometric errors allow us to deal with a photometry completeness of almost 100% at $g \leq 23.0$ mag for the outer cluster regions, where crowding effects are negligible (Dey et al. 2019).

The most recent values of the Galactic extinction are also available on the DR8 catalogs, from which we built the reddening map shown in Fig. 1. We computed the average for two circular regions, delineated in the figure by red circles with radii of 6′ and 30′, respectively. We obtained $\langle E(B - V)\rangle = 0.114 \pm 0.004$ mag and 0.117 ± 0.022 mag for the smallest and largest circles, respectively. These values show that differential reddening should not mislead our interpretation of the stellar density distribution around Pal 13.

The intrinsic (reddening corrected) cluster CMD is depicted in Fig. 2 (left panel) for all the measured stars distributed within the smallest red circle (see Fig. 1). We note that intrinsic g_o magnitudes and $(g - r)_o$ colors are available in the DR8 catalogs. As can be seen, the main cluster features –including some dispersion from field star contamination– are clearly distinguished. For comparison purposes, we built a reference intrinsic star field CMD from stars distributed within an annular region located far away from the cluster and with an area equal to that of the
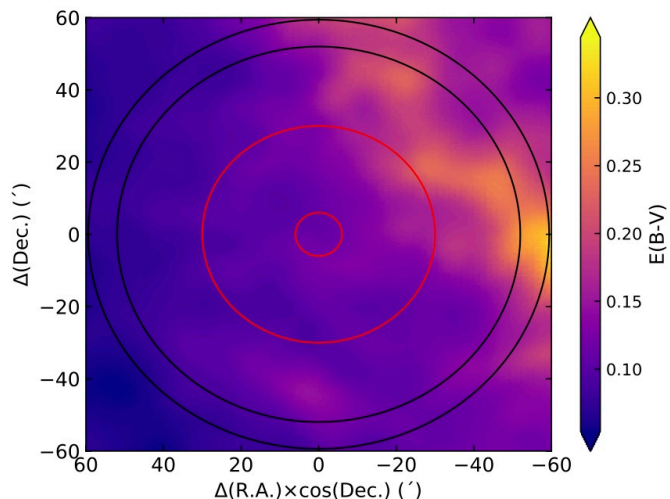
Fig. 1. Reddening map across the field of Pal 13. The red circles are of 6′ and 30′ in radius. The outer black annular region is of the same size as the largest red circular region.

smallest red circle (right panel of Fig. 2). This CMD reveals that the star field contamination in the cluster CMD should not hamper reliable tracing of the stellar density map in the outer cluster regions.

3. Stellar density map

It is well known that because of two-body relaxation, the less massive a star is, the further out into the cluster regions it can reach. Therefore, less-massive stars are candidates to cross the Jacobi radius and thus to populate the cluster extra-tidal regions (Carballo-Bello et al. 2012). In previous studies of the external regions of the globular clusters NGC 288 (Piatti 2018a) and NGC 6779 (Piatti & Carballo-Bello 2019), we used a strip along the cluster main sequence (MS), from underneath its MS turnoff down to 2 mag, to map the distribution of their stellar populations beyond their tidal radii. Those stars have low-enough masses to have been subject to tidal effects, as is therefore expected for their counterparts in Pal 13, particularly because Pal 13 is less massive than NGC 288 and NGC 6779 (Baumgardt et al. 2019).

Following the above recipe, we defined the area in the cluster CMD shown by the red contour in Fig. 2 (left panel) to build the respective stellar density map. This area comprises as many cluster MS stars as possible and minimizes the field star contamination (see right panel of Fig. 2). Nevertheless, we applied a procedure to get rid of field stars that fall inside the defined strip. The method was devised by Piatti & Bica (2012) and used satisfactorily for cleaning CMDs of star clusters projected towards crowded star fields (e.g., Piatti 2017b,c,a, and references therein) and affected by differential reddening (e.g., Piatti 2018b; Piatti et al. 2018, and reference therein). It relies on an accurate representation of the star field CMD in terms of its stellar density, luminosity function, and color distribution. This is done by considering the position of each field star in the cluster CMD and by subtracting the closest star in the cluster CMD to that field star. In doing this, we considered the uncertainties in magnitudes and colors by repeating the procedure hundreds of times with magnitudes and colors varying within their respective errors. For the designed MS strip, photometric errors increase from ≈0.01 mag up to 0.04 in g_o and from ≈0.01 mag up to 0.07 mag in $(g - r)_o$ for the range $g_o = 21-23$ mag.
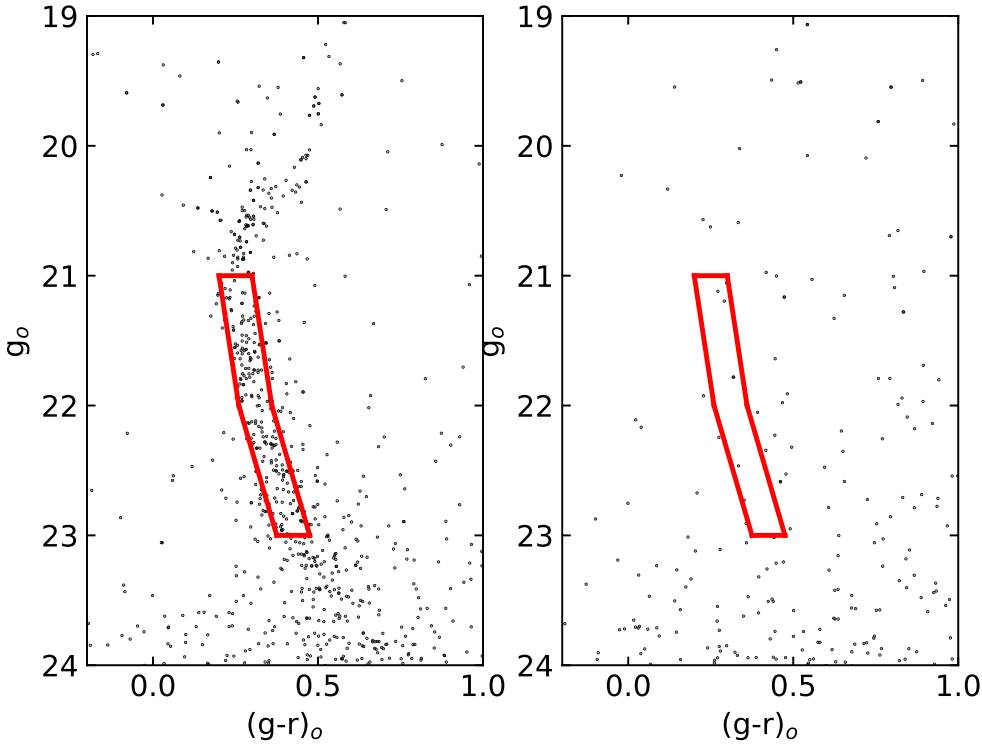
Fig. 2. Color–magnitude diagrams of stars in the field of Pal 13 ($r < 6'$; *left panel*) and in an annular region of similar area centered on the cluster with an outer radius of 60′ (*right panel*). The region along the cluster MS used to perform star counts is delineated with red contour lines.

As for the reference star field, we chose an annular region centered on the cluster and located relatively far away from the cluster, but not so far as to lose the star field characteristics in the direction toward the cluster. The chosen annulus is meant to include any possible star field population and reddening variation around Pal 13. The cleaned circular cluster area ($r < 30'$) and the star field annular region are of equal size. The latter is illustrated with black circles in Fig. 1.

From the resulting cleaned cluster CMD, we built the stellar density map for those stars spread within the boundaries of the defined MS strip and located inside a circle of radius $r = 30'$. We used a kernel density estimator (KDE) technique. Particularly, we employed the KDE routine within AstroML ([Vanderplas et al. 2012](#)). We superimposed a grid of 400×400 squared cells to the area of interest and used a range of values for the KDE bandwidth from 0.3′ up to 3′ in steps of 0.3′ in order to apply the KDE to each generated cell. The KDE technique was also used to estimate an optimal bandwidth of 1.5′, which means that we resolved structural details larger than approximately one-seventh of $r_t = 4.94'$ ([Baumgardt et al. 2019](#)). We also estimated the background level using the stars distributed within the annular region defined above (black circles in Fig. 1). We divided such an annulus into 16 adjacent sectors of 22.5° in width, where we counted the number of stars. We rotated such an array of sectors by 11.25° and repeated the star counting. Finally, we derived the mean value in the 32 defined sectors, which turned out to be 0.037 stars arcmin^{-2}. As for the standard deviation, we performed 1000 Monte Carlos realizations using the stars located beyond 10′ from the cluster center, which were rotated randomly (one different angle for each star) before recomputing the density map. The resulting standard deviation of all the generated density maps turned out to be 0.011 stars arcmin^{-2}.

The resulting observed and field-star-cleaned stellar density maps are depicted in the left and right panels of Fig. 3, respectively. The color scale represents the standard deviations over the mean value in the field, that is, $\eta = (\text{signal} - 0.037)/0.011$. We

have painted white stellar densities higher than 10η in order to highlight the cluster without the dense stellar structures. Every point used to generate the field-star-cleaned density map was also employed to build the cluster stellar radial profile shown in Fig. 4.

We additionally considered different star field regions distributed beyond 40′ from the cluster center and applied the same cleaning procedure for their respective MS strips using the same reference star field as for Pal 13 in all the executions. We found that the resulting cleaned stellar density maps do not contain any visible structure above 1η, which means that the residuals of the cleaning technique are negligible.

4. Analysis and discussion

The observed cluster MS strip stellar density map would seem to suggest the existence of a concentration of some number of stars from $\approx 5'$ out to $\approx 10'$ from the cluster center following an azimuthally irregular pattern (see Fig. 3, left panel). The lack of detection of further stellar densities that could be visibly associated to Pal 13 calls our attention to the previously derived larger r_t values: $14' < r_t < 26'$ ([Côté et al. 2002](#); [Bradford et al. 2011](#)). In this regard, we recall that field star contamination and incompleteness effects in star counts could lead to obtain meaningless [King (1962)](#)'s core and tidal radii.

Here we used a field-star cleaning procedure that has turned out to be effective in removing such contamination and in highlighting the intrinsic extra-tidal features of globular clusters projected on crowded fields or affected by differential reddening (e.g., [Piatti & Carballo-Bello 2019](#)). Particularly, Pal 13 would not seem to be projected on either a field affected by significant differential reddening (see Sect. 2) or on a crowded star field (see Fig. 2, right panel). From this point of view, the cluster is an easy target for our purposes, in addition to highlighting the effectiveness of the cleaning method even in more complicated cluster fields.
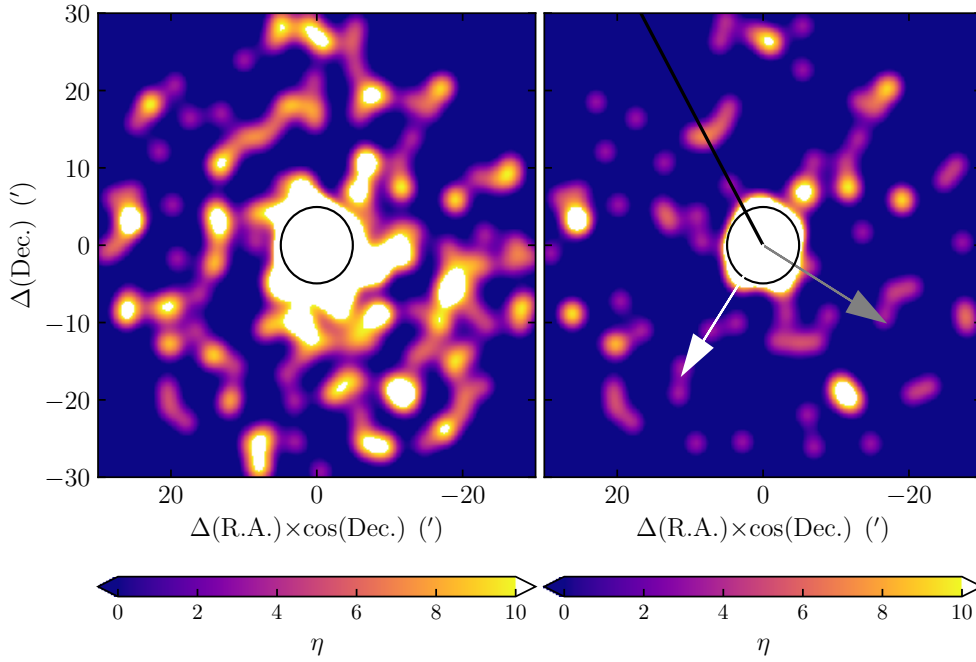
Fig. 3. Observed (*left panel*) and field-star-cleaned (*right panel*) stellar density maps, built from stars that occupy the MS strip defined in Fig. 2. The black circle centered on the cluster indicates the assumed tidal radius Baumgardt et al. (2019; 4.94′). The different arrows indicate the directions of the cluster proper motion (gray) and of the Galactic center (white). The black line represents the cluster orbit computed with GravPot16.
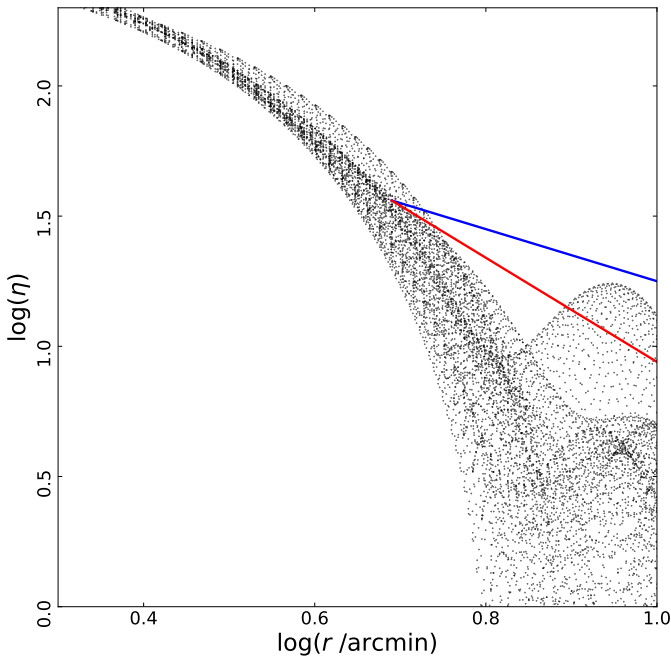

Fig. 4. Standard deviations over the mean value in the field as a function of the distance from the cluster center traced with every point generated using the KDE technique (see text for details). The blue and red lines correspond to a power law with $\alpha = 1$ and 2, respectively.

The resulting cleaned stellar density map shown in Fig. 3 (right panel) exhibits a more rounded shape than the observed one (Fig. 3, left panel), with some scattered stellar debris. The figure also shows an excess of stars above 3η beyond the adopted limiting radius $r_t = 4.94'$ ($\equiv$ Jacobi's radius; black circle in Fig. 3) obtained by Baumgardt et al. (2019) using Eq. (8) in Webb et al. (2013). We refer the reader to Piatti et al. (2019) for a discussion on the uncertainties of the globular cluster parameters derived by Baumgardt et al. (2019) from the integration of their orbital motions. Particularly, these latter authors estimated

a typical error of the Jacobi radius of 1.2′ at the Galactocentric distance of Pal 13. Figure 4 also illustrates the numbers given above.

We further analyzed the possibility of tidal deformations across the cluster stellar density map, in the sense that preferential orientation toward the Galactic center and along the direction of the orbit of the cluster are expected in the innermost and outermost parts, respectively (Montuori et al. 2007). We followed the recipe applied by Sollima et al. (2011) based on counts of cluster MS strip stars in alternate pairs of circular sectors of 90° in width located at a given distance from the cluster center and oriented at a position angle (PA) in opposite directions. We then computed the ratio $R(\mathrm{PA}) = (N_c^A N_f^B)/(N_c^A N_f^B)$, where A and B are the pair of alternate sectors, and c and f refer to the cluster MS strip and a CMD field rectangle defined by $21 < g_o(\mathrm{mag}) < 23$ and $1.5 < (g - r)_o(\mathrm{mag}) < 1.7$. In order to assess the statistical significance of our results, we performed 1000 Monte Carlo realizations using the same number of measured stars distributed randomly in PA and then obtained the mean and standard deviations of those independent executions. Figure 5 depicts the resulting curves. As can be seen, there are no noticeable tidal deformations across Pal 13. For completeness purposes we included in Fig. 3 (right panel) the directions toward the Galactic center and of the motion of the cluster. As for the globular cluster itself, extra-tidal extensions towards the SW and NE directions are marginally present around the cluster. Pal 13 has recently undergone a gravitational shock ($\sim$0.6 Gyr according to GravPot16), meaning that it is very likely that the extra-tidal extensions visible in Fig. 3 (right panel) correspond to a very recent disk-shock, with the extra-tidal material aligned in the tidal directions.

Some recent studies on the extended structures of globular clusters have found that at the outer regions the stellar density is $\propto r^{-\alpha}$, with α between 1 and 2 (e.g., Olszewski et al. 2009; Piatti 2017a). If we assumed a power-aw decrease of the stellar density for the outermost cluster region with a slope of $\alpha = 1$ and 2, we would find that Pal 13 vanishes down to 3η level at $\approx$59′ and 17′, respectively. The power-law profiles for $\alpha = 1$ and 2 are shown in Fig. 4 with blue and red lines, respectively. We note that the
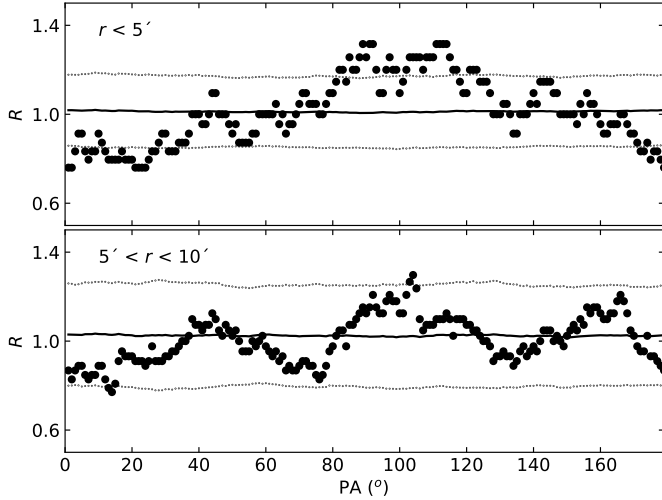
Fig. 5. Ratio $R = (N_c^A N_f^B)/(N_c^A N_f^B)$ (see Sect. 4 for detais) versus PA obtained from star counts in the star-field-cleaned MS strip (large filled circles). Solid and dotted lines represent the resulting mean and dispersion of the Monte Carlo simulations, respectively.

calculation of r_t involves the cluster over the course of its orbits, meaning that it varies from the perigalactic (9.04 ± 1.74 kpc) up to the apogalactic (67.48 ± 12.5 kpc) distances between 2.6′ and 7.2′, respectively (Piatti et al. 2019). This outcome suggests that its present extra-tidal population reaches ≈ 1.4 × r_t.

Recently, Piatti (2019) used the catalogs of Baumgardt et al. (2019) to investigate the kinematics of the Milky Way globular clusters. His results show that outer globular clusters are prone to more highly eccentric orbits (high eccentricity) than globular clusters moving in the Milky Way disk, regardless of the direction of their motions (prograde or retrograde orbits). The orbits of outer globular clusters also preferentially have large inclination angles. As far as accreted globular clusters are concerned, they show radial orbits independently of their position in the Galaxy. Globular clusters whose orbits have inclination angles ≲50° have experienced more disk crossings than those moving along more circular orbits in the disk at a similar Galactocentric distance. Therefore, they have lost more mass (Gnedin et al. 1999; Webb et al. 2014). Piatti et al. (2019) suggested that the lack of outer clusters rotating in nearly circular orbits (and at low inclination angles) could be due to their accreted origin, while the lack of such clusters in the inner Milky Way regions could be due to disruption.

According to Baumgardt et al. (2019), Pal 13 has a retrograde orbital motion ($V_\phi = -73.52$ km s^{-1}), an eccentricity of 0.76 ± 0.05, and an orbital inclination of 112.26° ± 6.26°. The ratio of the radial to total space velocity is 0.86 and the semi-major axis a (average between the perigalactic and apogalactic distances) is 38.26 ± 5.50 kpc, respectively. The ratio of the cluster mass lost due to Milky Way tidal disruption to the total initial cluster mass computed by Baumgardt et al. (2019) is 0.36, assuming that the cluster lost half of its initial mass via stellar evolution. All these features could favor an accreted origin for Pal 13. Indeed, Koposov et al. (2019) mention this cluster, alongside another six, as being located at $|\phi_2| < 7°$ from the great circle of the Orphan stream, whose progenitor could be a dwarf galaxy. On the other hand, Massari et al. (2019), using kinematics and chemical abundance information, assigned individual progenitors to most of the known Milky Way globular clusters, the Sequoia dwarf galaxy being the one associated to Pal 13. Koch & Côté (2019) also discuss this issue.

Küpper et al. (2011) and Balbinot & Gieles (2018) mention that the cluster is close to its apogalactic distance. Küpper et al. (2011) claimed that because of its position, the cluster should have experienced an expansion that could have encompassed any extra-tidal structure into the expanded body. Balbinot & Gieles (2018) found that cluster tails are more densely packed at apogalacticon, meaning that the cluster should be in the best condition possible for observability of its tails (extra-tidal features). From Baumgardt et al. (2019), Pal 13 is currently at a Galactocentric distance of 25.92 kpc, meaning that is 1.5 t farther from its apogalactic distance than from its perigalactic one (see also the cluster's orbit in Yepez et al. 2019). At that position, the cluster exhibits a moderately extended halo of low density. Furthermore, according to the above estimated r_t values, the extra-tidal corona would also be observed even at the apogalactic distance.

The presence of extra-tidal features in Pal 13 could alternatively be related to the relatively large estimated ratio of mass lost by tidal disruption (0.36). Hamren et al. (2013) showed that low-mass globular clusters may have lost a considerable amount of mass as compared to those more massive clusters. The left panel of Fig. 6 shows the ratio of the cluster mass disrupted by tidal effects to the total cluster mass as a function of the semi-major axis for the entire sample of globular clusters in Baumgardt et al. (2019). As can be seen, there is no clear correlation between the mass lost and the initial cluster mass for clusters at a similar semi-major axis to that of Pal 13, as suggested by Hamren et al. (2013). However, if we reproduce that plot using eccentricity as the color-scale variable, a clearer correlation arises, in the sense that the higher the orbital eccentricity of a globular cluster with similar semi-major axis to that of Pal 13, the higher the mass lost by tidal disruption. This outcome is in the line with the recent results of Piatti et al. (2019). Figure 1 of this latter publication shows that cluster eccentricity plays a role in the amount of cluster mass lost by tidal disruption, because of the more numerous disk crossings experienced with respect to clusters with more rounded orbital motions. Likewise, Fig. 1 suggests that present-day cluster-limiting radii, for clusters with similar semi-major axes, are smaller for those that have lost a larger amount of mass due to tidal effects, which we corroborate for Pal 13. These results are fully compatible with Pal 13 being relatively compact and at the same time exhibiting extra-tidal features.

5. Conclusions

In this work we take advantage of the DECaLS DR8 data sets to address the issue of the existence of extra-tidal structures around Pal 13, one of the relatively compact and less massive known Milky Way globular clusters. Precisely because of its size, some previous studies have concluded that the cluster does not extend beyond its Jacobi radius, and that the farthest low-mass members are quite distant from that boundary. However, these conclusions are a matter of debate, since complementary studies based on *Gaia* DR2 proper motions or surface stellar density profiles have found evidence suggesting the cluster is being tidally stripped. Additionally, there has been no consensus about its actual dimensions judging by the wide range of values derived for its tidal radius.

As far as we are aware, the Panoramic Survey Telescope and Rapid response System (Pan-STARRS PS1, Chambers et al. 2016) and DECaLS are the only present publicly available astrometric and photometric surveys covering a wide area around Pal 13, making them valuable tools for studying the cluster
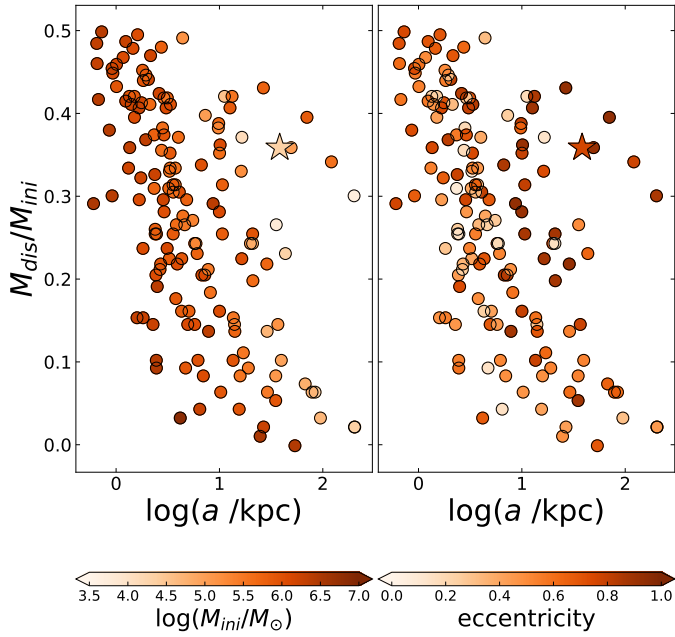
Fig. 6. Relationship between the ratio of the cluster mass lost by tidal effects to the initial cluster mass as a function of the cluster orbit semi-major axis for the entire sample of Milky Way globular clusters in the catalogs of Baumgardt et al. (2019). Symbols are colored according to the respective horizontal color bars. Pal 13 is represented by a large starred symbol.

extended structures. We decided to use DELCaLS DR8 because of its comparatively better performance in terms of limiting magnitude, photometric errors, and completeness. This data set was employed to build a stellar density map of stars distributed along the cluster MS, down to 2 mag below the MS turnoff.

At first glance, the cluster stellar density map shows almost smooth contours around the outer cluster regions that seem to reach out to approximately 1.6 t its limiting radius. Here, we adopted the most recent value of $r_t = 4.94'$ derived by Baumgardt et al. (2019) using line-of-sight velocity and proper motion velocity dispersion profiles fitted from a grid of dedicated N-body simulations. This outcome favors the presence of stars escaping the cluster, a phenomenon frequently seen in globular clusters that have crossed the Milky Way disk a large number of times (Piatti et al. 2019). Moreover, the high eccentricity and large inclination angle of the orbital motion of Pal 13 help us to speculate on that possibility. Furthermore, because of its retrograde direction of motion, Pal 13 has been suggested to have an accreted origin, which is found to associated to the Sequoia progenitor when its age and overall metallicity are also considered (Massari et al. 2019). A further six globular clusters could have been formed in the same dwarf galaxy, and four of them for which there have been studies of their external regions also have extra-tidal features.

References

Balbinot, E., & Gieles, M. 2018, MNRAS, 474, 2479
Barbá, R. H., Minniti, D., Geisler, D., et al. 2019, ApJ, 870, L24
Baumgardt, H., Hilker, M., Sollima, A., & Bellini, A. 2019, MNRAS, 482, 5138
Belokurov, V., Evans, N. W., Irwin, M. J., Hewett, P. C., & Wilkinson, M. I. 2006, ApJ, 637, L29
Belokurov, V., Erkal, D., Evans, N. W., Koposov, S. E., & Deason, A. J. 2018, MNRAS, 478, 611
Bradford, J. D., Geha, M., Muñoz, R. R., et al. 2011, ApJ, 743, 167
Carballo-Bello, J. A., Gieles, M., Sollima, A., et al. 2012, MNRAS, 419, 14
Carballo-Bello, J. A., Martínez-Delgado, D., Navarrete, C., et al. 2018, MNRAS, 474, 683
Chambers, K. C., Magnier, E. A., Metcalfe, N., et al. 2016, ArXiv e-prints [arXiv:1612.05560]
Correnti, M., Bellazzini, M., Dalessandro, E., et al. 2011, MNRAS, 417, 2411
Côté, P., Djorgovski, S. G., Meylan, G., Castro, S., & McCarthy, J. K. 2002, ApJ, 574, 783
Dey, A., Schlegel, D. J., Lang, D., et al. 2019, AJ, 157, 168
Fernández-Trincado, J. G., Beers, T. C., Placco, V. M., et al. 2019, ApJ, 886, L8
Gnedin, O. Y., Lee, H. M., & Ostriker, J. P. 1999, ApJ, 522, 935
Grillmair, C. J. 2019, ApJ, 884, 174

Hamren, K. M., Smith, G. H., Guhathakurta, P., et al. 2013, AJ, 146, 116
Harris, W. E. 1996, AJ, 112, 1487
Ibata, R. A., Bellazzini, M., Malhan, K., Martin, N., & Bianchini, P. 2019, Nat. Astron., 3, 667
Jordi, K., & Grebel, E. K. 2010, A&A, 522, A71
King, I. 1962, AJ, 67, 471
Koch, A., & Côté, P. 2019, A&A, 632, A55
Koposov, S. E., Belokurov, V., Li, T. S., et al. 2019, MNRAS, 485, 4726
Kunder, A., Bono, G., Piffl, T., et al. 2014, A&A, 572, A30
Kundu, R., Minniti, D., & Singh, H. P. 2019, MNRAS, 483, 1737
Küpper, A. H. W., Kroupa, P., Baumgardt, H., & Heggie, D. C. 2010, MNRAS, 401, 105
Küpper, A. H. W., Mieske, S., & Kroupa, P. 2011, MNRAS, 413, 863
Kuzma, P. B., Da Costa, G. S., Mackey, A. D., & Roderick, T. A. 2016, MNRAS, 461, 3639
Massari, D., Koppelman, H. H., & Helmi, A. 2019, A&A, 630, L4
Montuori, M., Capuzzo-Dolcetta, R., Di Matteo, P., Lepinette, A., & Miocchi, P. 2007, ApJ, 659, 1212
Myeong, G. C., Jerjen, H., Mackey, D., & Da Costa, G. S. 2017, ApJ, 840, L25
Myeong, G. C., Vasiliev, E., Iorio, G., Evans, N. W., & Belokurov, V. 2019, MNRAS, 488, 1235
Navarrete, C., Belokurov, V., & Koposov, S. E. 2017, ApJ, 841, L23
Niederste-Ostholt, M., Belokurov, V., Evans, N. W., et al. 2010, MNRAS, 408, L66
Odenkirchen, M., Grebel, E. K., Dehnen, W., et al. 2003, AJ, 126, 2385

Olszewski, E. W., Saha, A., Knezek, P., et al. 2009, AJ, 138, 1570
Piatti, A.E. 2017a, ApJ, 846, L10
Piatti, A.E. 2017b, ApJ, 834, L14
Piatti, A.E. 2017c, MNRAS, 465, 2748
Piatti, A.E. 2018a, MNRAS, 473, 492
Piatti, A.E. 2018b, MNRAS, 477, 2164
Piatti, A. E. 2019, ApJ, 882, 98
Piatti, A. E., & Bica, E. 2012, MNRAS, 425, 3085
Piatti, A. E., & Carballo-Bello, J. A. 2019, MNRAS, 485, 1029
Piatti, A. E., Cole, A. A., & Emptage, B. 2018, MNRAS, 473, 105
Piatti, A. E., Webb, J. J., & Carlberg, R. G. 2019, MNRAS, 489, 4367
Shipp, N., Drlica-Wagner, A., Balbinot, E., et al. 2018, ApJ, 862, 114
Siegel, M. H., Majewski, S. R., Cudworth, K. M., & Takamiya, M. 2001, AJ, 121, 935
Sollima, A., Martínez-Delgado, D., Valls-Gabaud, D., & Peñarrubia, J. 2011, ApJ, 726, 47
Sollima, A., Martínez Delgado, D., Muñoz, R. R., et al. 2018, MNRAS, 476, 4814
Vanderbeke, J., De Propris, R., De Rijcke, S., et al. 2015, MNRAS, 450, 2692
Vanderplas, J., Connolly, A., Ivezić, Ž., & Gray, A. 2012, Conference on Intelligent Data Understanding (CIDU), 47
Webb, J. J., Harris, W. E., Sills, A., & Hurley, J. R. 2013, ApJ, 764, 124
Webb, J. J., Sills, A., Harris, W. E., & Hurley, J. R. 2014, MNRAS, 445, 1048
Yepez, M.A., Arellano Ferro, A., Schröder, K.P., et al. 2019, New Astron., 71, 1